Letters in High Energy Physics
ISSN: 2632-2714
Volume 2025

Heat Transfer by Non-Newtonian-Based SWCNT-Nanofluids in the Presence of MHD

Mohamed Azizou[1,*], Saleh Khir[2], Mounir Zirari[1,2,3], Mohamed Nadjib Bouaziz[1,3], and Redha Rebhi[1,2]

[1]*Department of Mechanical Engineering, University of Medea, Medea 26000, Algeria.*
[2]*LERM-Renewable Energy and Materials Laboratory, University of Medea, Medea 26000, Algeria.*
[3]*Biomaterials and Transport Phenomena Laboratory (LBMPT), University of Yahia Fares, Medea, 26000, Algeria*.

Corresponding author*:azizou.mohamed@univ-medea.dz **Received:** 22-12-2024 **Published:** 23-02-2025

Abstract

This paper presents a numerical investigation of heat transfer involving non-Newtonian-based nanofluids within an inclined square porous medium under the influence of MHD. To analyze the behavior of non-Newtonian fluids, the power-law model, a widely used rheological model for studying flow phenomena in porous media, was employed. The Darcy model is utilized to describe the flow within the porous medium. The problem is characterized by a set of interrelated non-linear differential equations, known as governing equations, which consist of the mass conservation equation (also called the continuity equation), the momentum equation, and the energy equation. These core governing equations are solved numerically using the finite difference method, with convective flow in porous media modeled through Darcy's law and the Boussinesq approximation. The main parameters influencing the problem are the Rayleigh number (R_T), the power-law index (n), the volume fraction of nanoparticlesϕ, the inclination angle of the applied magnetic field (ω), the Hartmann number (Ha), and the inclination angle of the cavity (Φ). The results show that the power-law index (n), the volume fraction of nanoparticlesϕ, inclination angle (Φ), and Hartmann number (Ha) have a significant impact on the flow intensity, as well as on the heat transfer driven by natural convection within the enclosure.

Keywords: SWCNT-Nanofluids, non-Newtonians, porous media, MHD, power law model.

1. Introduction

Transport phenomena in porous media have received considerable attention over the past few decades due to their importance in numerous technical and industrial applications. These applications include thermal insulation, fixed-bed heat exchangers, drying technology, catalytic reactors, petroleum industries, geothermal systems, and electronic cooling [1, 2]. Furthermore, substantial progress has also been made in the use of porous media in biomedical applications such as tissue replacement production, drug delivery, advanced medical imaging, porous scaffolds for tissue engineering, and transport in biological tissues [3, 4]. In industrial processes, another method to enhance convective heat transfer characteristics is to use a porous medium (any material consisting of a solid matrix with interconnected voids is called a porous medium, such as rocks and open-cell aluminum foams, Nield and Bejan [5]) and a nanofluid.

Nanofluids are colloidal mixtures of nanoparticles (ranging from 1 to 100 nm) suspended in a base fluid. The nanoparticles can be metallic, non-metallic, oxide, carbide, ceramic, carbon-based, a mixture of different nanoparticles (hybrid nanoparticles), or even nanometer-scale liquid droplets. The base fluid can be a low-viscosity liquid such as water, a refrigerant, or a high-viscosity liquid such as ethylene glycol, mineral oil, or a mixture of different types of liquids (e.g., EG+water, water+propylene glycol, etc.). The term "nanofluid" was first coined by Stephen Choi [6]. Few researchers have observed in their studies that the addition of nanoparticles to conventional fluids significantly improves their thermal conductivity [7–10] compared to base fluids. Saidur et al. [11] observed that the thermal conductivity of nanofluids increased with the rise in the volumetric concentration of particles in the base fluid. The mixing of nanoparticles with the base fluid can alter the thermophysical properties of the fluids because nanoparticles have a higher thermal conductivity than the base fluids, Wang and Mujumdar [12]. However, various experiments have shown that the increase in thermal conductivity could be offset by an increase in viscosity, and they have observed a slight penalty in terms of pressure loss [13, 14]. Tiwari et al. [15, 16] observed that an increase

in the volumetric concentration of nanoparticles increased the viscosity and density of the fluid, which in turn caused a pressure drop and consequently increased the pumping power. Vajjha and Das [17] observed that an increase in the nanoparticle load in the base fluid significantly increased the viscosity and density.

In many practical environmental, industrial, and geophysical applications, working fluids exhibit non-Newtonian behavior, meaning their viscosity is not constant but depends on the shear rate. This introduces additional complexities compared to Newtonian fluids, Chhabra and Richardson [18]. Non-Newtonian fluids, that is, those that do not follow Newton's viscosity law, have been widely used in many industries such as food, petrochemicals, pharmaceuticals, etc. Regarding rheology, non-Newtonian fluids can be classified into Bingham plastic fluids, pseudoplastic fluids, and dilatant fluids. Furthermore, models of non-Newtonian fluids can be divided into time-dependent, time-independent, and viscoelastic models [19, 20].

Magnetic fields are used in drying and lubrication technologies, food cleaning, float glass production, control of hydrodynamic behavior during float glass production processes, solidification, and crystal growth. Moreover, the applications of magnetic fields to nanofluid flows are gaining increasing interest due to their wide use in many technological applications such as nuclear reactor coolers, plasma, molten metal purification, and metalworking processes, where convection is controlled by an external magnetic field (magnetohydrodynamics, or MHD), Minea [21]. Mansour et al. [22] presented a numerical study on free MHD convection in an inclined square cavity with a heat source. They revealed that the Nusselt number takes a high value in the presence of a magnetic field. In another study by Bühler et al. [23], they discovered that adding nanoparticles to the base fluid improved the convection rate, and that an increase in the Hartmann number decreased the average Nusselt number. A numerical study on the description of liquid metal flows in a capillary porous system under the influence of a uniform external magnetic field. They concluded that MHD liquid metal flows in porous media depend on the electrical properties of the porous material and the orientation and strength of the magnetic field. Another review published by M'hamed et al. [24] on the application of an external magnetic field to nanofluids was published to address the question of why researchers apply external magnetic fields to nanofluids. They concluded that the applied external magnetic field affects the control of the flow characteristics of nanofluids rather than enhancing their thermal conductivity. The effect of the tilt angle and magnetic field on free convection in a porous cavity saturated with a nanofluid was studied by Nithyadevi and Rajarathinam, [25] they recorded a decrease in the heat transfer rate with the increase in the Hartmann number.

Jahanbakhshi et al. [26] studied the influence of the magnetic field on the natural convection of a non-Newtonian fluid in an L-shaped cavity. Pirmohammadi and Ghassemi, [27] numerically studied natural convection in an inclined enclosure with a magnetic field. Their results indicated that increased Hartmann numbers lead to a reduction in convective heat transfer. The impact of magnetic field intensity on fluid flow and heat transfer in a cavity with inclined walls was studied numerically by Revnic et al. [28] Their results highlight the changes in the streamlines and isotherms due to the magnetic field.

Wang et al. [29] published a paper on the 3D free convection of liquid metal in a rectangular cavity under the influence of a magnetic field. They found that the heat transfer rate decreases under the effect of the magnetic field. Shankar et al. [30] provided a study on the stability of free convection of magnetohydrodynamic fluid in a saturated porous channel; they concluded that the magnetic field has a stabilizing effect on the stabilities of both the steady and oscillatory modes. Another paper was published by Sheikholeslami [31] on the flow of MHD CuO-H2O nanofluids in a porous channel using the mesoscopic method, and it was found that increasing the Hartmann number improves the heat transfer rate but reduces the flow velocity.

The heat transfer performance and irreversibility production of free convection of non-Newtonian nanofluids in a square enclosure with the presence of a horizontal magnetic field were studied by Kefayati [32], considering the impact of ϕ, Ra, Ha, and n. Heat transfer and irreversibility production were influenced by nanoparticles at different values of Ra and n. However, an increase in Ha reduced heat transfer and irreversibility production, which further decreased with the growth of n. Heat transfer and the flow of a non-Newtonian fluid in a cavity with a sinusoidal heated wall and a magnetic field under free convection are discussed by Kefayati [33]. The study was conducted at different values of Ra, Ha, n, and the

magnetic field tilt angle. The flow and heat transfer performance were influenced by the magnetic field in both vertical and horizontal directions. The vertical magnetic field improved heat transfer performance at $Ra = 10^5$.

Free convection of nanofluid in an enclosure, with one side having a sinusoidal temperature distribution, under the impact of the magnetic field was studied by Kefayati [34]. The hydrothermal characteristics of the nanofluid in a U-shaped enclosure subjected to a non-Newtonian force and exposed to a magnetic field are analyzed in detail using the Galerkin finite element method. A comprehensive analysis is conducted to explore the influence of $, Ha, AR,$ the magnetic tilt angle, ϕ, and n on the performance characteristics was studied by Ali et al. [35].

Aboud et al. [36] studied the effect of MHD on mixed convection in a circular annular enclosure filled with non-Newtonian nanofluid. They concluded that in the absence of a magnetic field, the streamlines and isotherms have circular shapes for all values of the Richardson number and the low power-law index. At a specific value of the power-law index, the strength of the magnetic field alters the fluid flow behavior by modifying the pattern of streamlines and the values of the stream function. The effect of the power-law index on the stream function decreases with the increase in the magnetic field intensity. At Ri = 0.01 and 0.001, the heat transfer and the local Nusselt number decrease with the increase in the volume fraction. The increase in magnetic field intensity enhances the influence of nanoparticles on improving heat transfer compared to $Ha = 0$. The average Nusselt number increases with the Hartmann number, but the trend differs with each value of the Hartmann number and the power-law index.

In a study by Motozawa et al. [37], the effect of the magnetic field on heat transfer in a flow through a rectangular duct was investigated. The results of their work showed that in the presence of a magnetic field, the local heat transfer coefficient increased by 20% in the horizontal square-section channel under an external magnetic field perpendicular to the direction of the nanofluid flow at a Reynolds number of 780.

Javadpour et al. [38] presented an experimental study on forced convection heat transfer and the friction factor of a non-Newtonian nanofluid flow through a ring in the presence of a magnetic field.

Natural convection of nanofluids in the presence of MHD in square enclosures has been examined, and most studies are based on the numerical approach with very few on the experimental method. It has been observed that the improvement in heat transfer deteriorated with the presence of a magnetic field, except in a few cases where it increased at certain values. However, the experimental method showed an improvement in heat transfer when nanofluids were exposed to magnetic sources, which was further enhanced with an increase in magnetic strength. Furthermore, the increase in θ and Da was found to primarily enhance heat transfer in the cavities, while attenuation was mainly reported for an increase in γ. These results were strongly dependent on several variables, such as the orientation and application of thermal boundary conditions, the type and orientation of magnetic fields, the use, type, and number of heaters, temperature distribution methods, and the exposure of nanofluids to radiation effects and viscous dissipation. Additionally, several future research directions were identified in this work, Giwa et al. [39].

Another paper was published by Kefayati [40] on the FDLBM simulation of mixed convection in a cavity with a lid, filled with a non-Newtonian nanofluid in the presence of a magnetic field. They concluded that an increase in the power-law index reduces heat transfer at different Richardson and Hartmann numbers. The addition of nanoparticles increases heat transfer for various power-law indices, Hartmann numbers, and Richardson numbers.

Kumar and Srinivas [41] conducted a study on pulsating flow of a non-Newtonian nanofluid in a porous channel with a magnetic field. The results indicate that the velocity of the nanofluid decreases with an increase in the Hartmann number. The temperature of the nanofluid increases with a given increase in the volume fraction of nanoparticles, the radiation parameter, and the heat source parameter, while it decreases with an increase in the Hartmann number. Furthermore, it is observed that the heat transfer rate at the lower wall increases with the increase in the volume fraction of nanoparticles and with the increase in the heat source.

Bennia et al. [42] conducted a study on CFD modeling of forced turbulent convection heat transfer and the friction factor in a tube for the magnetic nanofluid Fe_3O_4 in the presence of a magnetic field. The results obtained indicate that heat transfer and the friction

factor depend on the increase in the magnetic field, electrical conductivity, and volume fraction.

Recently, Alilat et al. [43]. published a paper on the inertial effects on natural hydromagnetic convection in an inclined rectangular porous medium saturated with SWCNT water nanofluids. Another study by Alilat et al. [44], conducted focused on improving the thermal convection in a Dupuit–Darcy model of a porous medium saturated with non-Newtonian SWCNT-water nanofluids. They concluded that heat transfer by convection favors the decrease of Carreau-Yasuda parameters a and$s$, and the increase of the time constant parameter E. The power-law index n of the Carreau–Yasuda model has a significant effect on the apparent viscosity, the fluid flow intensity, and consequently on the convection rate. The more the fluid exhibits shear-thinning behavior (decrease in n), the better the convection rate. Additionally, the influence of the inclination angle and the percentage of SWCNT on the convection rate is also significant. Khir et al. [45, 46]. Conducted a study of Bistability Analysis in Double-Diffusive Convection within an Inclined rectangular and Square Porous Cavity Filled with a Power-Law Non-Newtonian Fluid.

The aim of this study is to investigate the influence of the power law index, Rayleigh number, Hartman number and SWCNT volume fraction on the free convection of SWCNT-water nanofluid filling an inclined square porous enclosure. Based on the literature reviewed, this research focuses on the free convection of non-Newtonian SWCNT-water nanofluid in a square porous enclosure, using the Darcy model to describe the flow in the porous medium, as well as the Darcy model taking into account the presence of a magnetic field.

2. Problem definition and mathematical formulation

As illustrated in Figure 1, a two-dimensional inclined porous cavity filled with a SWCNT-water non-Newtonian nanofluid is considered in the present, under the influence of an applied magnetic field. The cavity, of height H', is inclined at an angle Φ with respect to the horizontal axis. The top and bottom walls of the cavity are isothermally maintained at temperatures T'. The side walls of the cavity are assumed to be adiabatic. x' and y' denote the Cartesian coordinates, and a uniform and constant magnetic field $\vec{B}_0'$ is imposed at an inclination angle ω.

The study models a non-Newtonian SWCNT–water nanofluid in a homogeneous, isotropic porous medium under the Boussinesq approximation, with viscosity governed by the power-law model. Effects like radiation, Joule heating, and viscous dissipation are neglected.

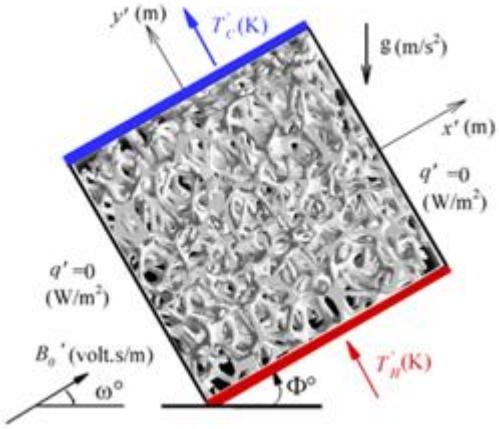

Fig. 1. Sketch of the cavity's coordinate system and boundary conditions.

In light of the previously stated assumptions, the following equations elucidate the conservation principles of mass, momentum, and energy:

$$\nabla.\vec{V'} = 0 \tag{1}$$

$$\frac{\mu'_{nf}}{K}\vec{V'} = -\nabla p' - \rho_{nf}\,\vec{g} + \vec{J'} \times \vec{B}_0' \tag{2}$$

$$\frac{\partial T'}{\partial t'} + \vec{V'}.\nabla T' = \alpha_{nf}\nabla^2 T' \tag{3}$$

$$\nabla.\vec{J'} = 0 \tag{4}$$

$$\vec{J'} = \sigma\left(-\nabla\vartheta' + \vec{V'} \times \vec{B}_0'\right) \tag{5}$$

In the present analysis, $\vec{V'}$ signifies the velocity vector, $p'$the pressure, $\vec{g}$ the gravitational acceleration vector, $\vec{j'}$ the electric current, α_{nf} the thermal diffusivity of the nanofluid-saturated porous medium, μ'_{nf} the apparent viscosity of the nanofluid, and t is the time. The permeability of the porous medium, K, the electrical conductivity, σ, the electric potential, ϑ', and the associated electric field, $-\nabla\vartheta'$.

As Garandet et al. [47] explained, in a 2D situation, Eqs. (4) and (5) simplifies to $\nabla^2\vartheta' = 0$. Due to the existence of an electrically insulating boundary

surrounding the enclosure, the unique solution is $\nabla\vartheta' = 0$.

The changes in density caused by buoyancy are described using the Boussinesq approximation (Tiwari and Das, [48]).

$$\rho_{nf} = \rho_{nf,0}\left[1-\left(\beta_T'\right)_{nf}\left(T'-T_0'\right)\right] \tag{6}$$

Here, T_0' and $\rho_{nf,0}$ denote the reference temperature and mass density, respectively. $(\beta_T')_{nf}$ represents the thermal expansion coefficient of the nanofluid.

Upon eliminating the pressure term from the momentum equations, the governing equations can be expressed as follows:

$$\mu_{nf}'\left[\frac{\partial v'}{\partial x'}-\frac{\partial u'}{\partial y'}\right]+\left[v'\frac{\partial \mu_{nf}'}{\partial x'}-u'\frac{\partial \mu_{nf}'}{\partial y'}\right]=$$
$$Kg\rho_{nf,0}\left(\beta_T\right)_{nf}\left[\frac{\partial T'}{\partial x'}\cos\Phi-\frac{\partial T'}{\partial y'}\sin\Phi\right]+ \tag{7}$$
$$K\sigma_{nf}B_0'^2\left[\begin{array}{l}\frac{\partial u'}{\partial x'}\cos\omega\sin\omega-\frac{\partial v'}{\partial x'}\cos^2\omega-\\ \frac{\partial v'}{\partial y'}\cos\omega\sin\omega+\frac{\partial u'}{\partial y'}\sin^2\omega\end{array}\right]$$

$$\frac{\partial T'}{\partial t'}+u'\frac{\partial T'}{\partial x'}+v'\frac{\partial T'}{\partial y'}=\alpha_{nf}\nabla^2T' \tag{8}$$

The properties of the nanofluid, including its densityρ_{nf}, thermal expansion coefficient$(\rho\beta_T')_{nf}$, and heat capacitance $\left(\rho C_p\right)_{nf}$ are determined using the nanofluid model proposed by Tiwari and Das [48], as expressed by the following equations:

$$\begin{aligned}\rho_{nf} &= \left(1-\phi\right)\rho_f+\phi\rho_p,\\ \left(\rho\beta_T'\right)_{nf} &= \left(1-\phi\right)\left(\rho\beta_T'\right)_f+\phi\left(\rho\beta_T'\right)_p,\\ \left(\rho C_p\right)_{nf} &= \left(1-\phi\right)\left(\rho C_p\right)_f+\phi\left(\rho C_p\right)_p\end{aligned} \tag{9}$$

The thermal conductivity k_{nf} of the nanofluid is determined using the model proposed by Xue [49].

$$k_{nf} = k_f\left[\frac{1-\phi+2\phi\frac{k_{CNT}}{k_{CNT}-k_f}\ln\left(\frac{k_{CNT}+k_f}{2k_f}\right)}{1-\phi+2\phi\frac{k_f}{k_{CNT}-k_f}\ln\left(\frac{k_{CNT}+k_f}{2k_f}\right)}\right] \tag{10}$$

The electrical conductivity of the nanofluid is determined based on the Maxwell [50] model and is expressed as:

$$\frac{\sigma_{nf}}{\sigma_f} = 1+\frac{3\left(\chi-1\right)\phi}{\left(\chi+2\right)-\left(\chi-1\right)\phi} \tag{11}$$

Here, $\chi = \sigma_p/\sigma_f$ represents the electrical conductivity ratio, ϕ denotes the volume fraction of nanoparticles, and the subscripts, p, and CNT correspond to the fluid (nano), particle, and carbon nanotube, respectively.

The thermophysical properties of SWCNT nanoparticles and water are summarized in Table 1.

Table 1. Thermophysical properties of Water, and Single-Wall Carbon Nanotubes (SWCNT).

Physical properties	water	SWCNT
$C_p(J.Kg^{-1}.K^{-1})$	4179	425
$\rho(Kg.m^{-3})$	997.1	2600
$k(W.m^{-1}.K^{-1})$	0.613	6600
$\beta\times10^{-5}(K^{-1})$	1.47	1.6
$\sigma(\Omega^{-1}m^{-1})$	21	4.8×10^{-7}

The apparent viscosity of the non-Newtonian SWCNT–water nanofluid, μ_{nf}', is determined using the following equation, as presented by Kefayati [32] and Jain and Bhargava [51]:

$$\mu_{nf}' = \frac{\mu_f'}{\left(1-\phi\right)^{2.5}} \tag{12}$$

Here, μ_f'represents the viscosity of the base fluid, characterized by the power-law model as described by Pascal [52, 53] as following:

$$\begin{aligned}\mu_f' &= \varepsilon\left(u'^2+v'^2\right)^{(n-1)/2},\\ \varepsilon &= 2h\Big/8^{(n+1)/2}\left(K\varphi\right)^{(n-1)/2}\left(n/\left(1+3n\right)\right)^n\end{aligned} \tag{13}$$

In this context, ε is a parameter in the power-law model, where φ and K represent the porosity and permeability of the porous medium, respectively, while h denotes the consistency index and n is the power-law index.

Equations (7), (8) and (12) are expressed in dimensionless form by introducing a new set of variables as follow:

$$(x,y)=(x',y')/H',\quad (u,v)=(u',v')H'/\alpha_f,$$
$$t=t'\alpha_f/H'^2, T=(T'-T_0')/\Delta T', \tag{14}$$
$$\mu_{nf}=h/\varepsilon(\alpha_f/H')^{n-1}$$

The dimensionless stream function, denoted asΨ, is defined as follows:

$$u=\frac{\partial\Psi}{dy},\quad v=-\frac{\partial\Psi}{dx} \tag{15}$$

By utilizing the previously outlined equations, the dimensionless equations governing the convective flow are presented as follows:

$$\mu_{nf}\left[\frac{\partial^2\Psi}{\partial y^2}+\frac{\partial^2\Psi}{\partial x^2}\right]+\left[\frac{\partial\Psi}{\partial y}\frac{\partial\mu_{nf}}{\partial y}+\frac{\partial\Psi}{\partial x}\frac{\partial\mu_{nf}}{\partial x}\right]=$$
$$-R_T H(\phi)\left(\frac{\partial T}{\partial x}\cos\Phi-\frac{\partial T}{\partial y}\sin\Phi\right)-Ha^2C(\phi) \tag{16}$$
$$\left[2\frac{\partial^2\Psi}{\partial x\partial y}\cos\omega\sin\omega+\frac{\partial^2\Psi}{\partial x^2}\cos^2\omega+\frac{\partial^2\Psi}{\partial y^2}\sin^2\omega\right]$$

$$E(\phi)\left(\frac{\partial^2T}{\partial x^2}+\frac{\partial^2T}{\partial y^2}\right)=\frac{\partial T}{\partial t}+\frac{\partial\Psi}{\partial y}\frac{\partial T}{\partial x}-\frac{\partial\Psi}{\partial x}\frac{\partial T}{\partial y} \tag{17}$$

$$\mu_{nf}=\left[\left(\partial\Psi/\partial x\right)^2+\left(\partial\Psi/\partial y\right)^2\right]^{(n-1)/2}\Big/\left(1-\phi\right)^{2.5} \tag{18}$$

From Eqs. (16) and (17), several parameters are clearly identified, including the Rayleigh number R_T, the Hartmann number Ha, $C(\phi)$, $H(\phi)$, and $E(\phi)$, which are expressed as follows:

$$\begin{cases} R_T=\dfrac{K\rho g\beta_T'\Delta T'(H'/\alpha_f)^n}{\varepsilon},\quad Ha=B_0'\sqrt{\dfrac{K\sigma_f}{\varepsilon(\alpha_f/H')^{n-1}}} \\ H(\phi)=1-\phi+\phi\dfrac{(\rho\beta_T')_p}{(\rho\beta_T')_f},\quad C(\phi)=1+\dfrac{3(\chi-1)\phi}{(\chi+2)-(\chi-1)\phi} \\ E(\phi)=\dfrac{k_{nf}}{k_f}\dfrac{(\rho C_p)_f}{(1-\phi)(\rho C_p)_f+\phi(\rho C_p)_p} \end{cases} \tag{19}$$

The hydrodynamic and thermal boundary conditions applied to the system's walls are presented in their dimensionless form as follows:

$$u=\Psi=0 \quad \text{at} \quad x=\pm\frac{1}{2},\ \text{and}\ v=\Psi=0 \quad \text{at} \quad y=\pm\frac{1}{2} \tag{20}$$

$$T=\pm\frac{1}{2} \quad \text{at} \quad y=\pm\frac{1}{2},\ \text{and} \quad \frac{\partial T}{\partial x}=0 \quad \text{at} \quad x=\pm\frac{1}{2} \tag{21}$$

The local and average Nusselt numbers, denoted as Nu_x, Nu_m, respectively, are given by:

$$Nu_x=-\frac{k_{nf}}{k_f}\frac{\partial T}{\partial y}\bigg|_{y=\pm1/2} \tag{22}$$

$$Nu_m=\int_{-1/2}^{+1/2}Nu_x dx \tag{23}$$

3. Numerical solution

The finite difference method with a uniform grid size is utilized to numerically solve the governing equations (16)-(17) and the boundary conditions equations (20)-(21). A second- order centered technique is used to discretize the energy and concentration equations. Two tri-diagonal matrix systems are produced for resolution at each time increment using Peaceman and Rachford's [54] alternating directions implicit method (ADI). One of these matrix systems results from implicit discretization in the x-direction, while the other comes from implicit discretization in the y-direction. The over relaxation method (S.O.R.) was utilized to solve the momentum equation, Eq. (16). Considering steady-state solutions, convergence is achieved when the following equation is satisfied:

$$\frac{\sum_i\sum_j\left|\Psi_{i,j}^{k+1}-\Psi_{i,j}^{k}\right|}{\sum_i\sum_j\left|\Psi_{i,j}^{k}\right|}\le10^{-6} \tag{24}$$

In this context, $\Psi_{i,j}^{k}$ represents the stream function value at the node (i,j) in the k^t iteration.

The effect of mesh size on the maximum absolute value of the stream function Ψ_0; at the center of the cavity, the average Nusselt number of the hot wall, and the apparent viscosity of the non-Newtonian nanofluid was tested for grid sizes ranging from 40× 40 to 120 × 120, as shown in Table 2. The tests revealed that a 100 × 100 grid is sufficient to accurately simulate the resolved equations while minimizing computational time.

Table 2. Convergence tests for specified parameters, $A = 1$, $Ha = 1$, ϕ=0.05, R_T=200, Φ=0°, and ω=0°, and different power-law index, n.

		Numerical solution				
Grids		**40×40**	**60×60**	**80×80**	**100×100**	**120×120**
n = 0.6	Ψ_0	13.668	13.944	14.065	14.108	14.135
	Nu_L	10.154	10.632	10.827	10.897	10.930
	μ_{nf}	6.124	6.786	7.365	7.890	8.373
n = 1.0	Ψ_0	6.456	6.458	6.458	6.458	6.458
	Nu_L	4.397	4.389	4.384	4.381	4.379
	μ_{nf}	1.136	1.136	1.136	1.136	1.136
n = 1.4	Ψ_0	3.770	3.775	3.778	3.781	3.782
	Nu_L	2.763	2.767	2.770	2.772	2.773
	μ_{nf}	0.685	0.604	0.552	0.514	0.485

To validate the accuracy of the current numerical solutions, Tables 3 and 4 presents the obtained numerical results,including the center stream function,Ψ_0 , value, as well as the average Nusselt, Nu, and Hartman Ha, numbers. A comprehensive comparison with the findings reveals a very good level of agreement especially Table 4.

Table 3. Comparison of average Nusselt number with previous numerical results for Ha = 0, ϕ = 0, and Φ = 90° and $n = 1$.

R_T	10	100	1000	
	Nu_L		Nu_L	Ψ_0
Walker and Homsy [55]	---	3.097	12.96	---
Bejan [56]	---	4.20	15.8	---
Beckermann et al. [57]	---	3.113	---	---
Gross et al. [58]	---	3.141	13.448	---
Moya et al. [59]	1.065	2.801	---	---
Manole and Lage [60]	---	3.118	13.637	---
Baytas and Pop [61]	1.079	3.16	14.06	---
Nawaf and Pop [62]	---	---	13.442	20.489
Alilat et al. [43]	1.079	3.113	13.770	20.457
Present results	1.079	3.120	13.586	20.374

Table 4. Comparison of Ψ_0, and Nu_L with previous numerical studied of Alilat et al. [43] for$R_T = 200$, $\phi = 0.05$, $\Phi = 90°$ and ω = 0° with various values of Ha.

Ha		Alilat et al. [43]	Present study
0	Ψ_0	8.323	8.323
	Nu_L	5.330	5.338
5	Ψ_0	0.974	0.968
	Nu_L	2.004	1.996
10	Ψ_0	0.255	0.255
	Nu_L	1.912	1.911

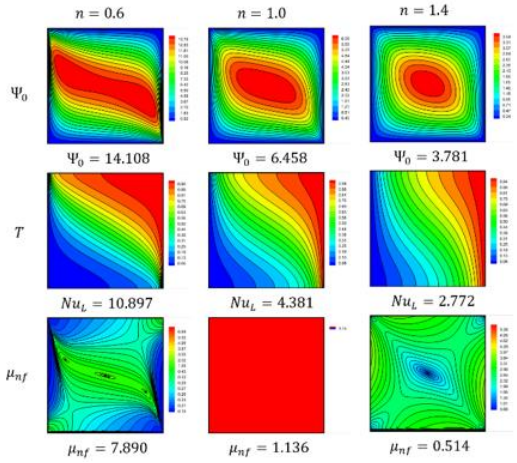

Fig 2. Contours of streamlines,Ψ_0, temperature, T, and nanofluid viscosity,μ_{nf}, for R_T =200, ϕ =0.05 Ha=1.0, Φ = 90°, ω = 0° and various values of n.

Figure 2 present the contours of streamlines, Ψ, temperature, T,and apparent viscosity of nanofluid, μ_{nf}, obtained numerically, for power-law index of n = 0.6 and 1.4 and for a Newtonian fluid (n = 1), at R_T = 200, ϕ=0.05 Ha=1.0, Φ = 90°, ω = 0°. The streamlines are uniformly distributed with designated increments, spanning from zero at the boundaries to the maximum value at the center. The isotherms are uniformly distributed between the successive positions of the peak temperature T_{max} situated lower edge of the right vertical wall. On the other hand, the minimum temperature T_{min} are situated along the upper edge of the left vertical wall. The apparent viscosity lines are uniformly distributed with specified increments $\Delta\mu_{nf}$ between the minimum value of apparent viscosity ($\mu_{\text{nf}min}$) in the cavity edges and the extremum value of apparent viscosity,($\mu_{\text{nf}max}$), on the center of cavity when n = 0.6, this is the opposite of n = 1.4, and it's clearly constant (μ_{nf} =1) when $n = 1$.

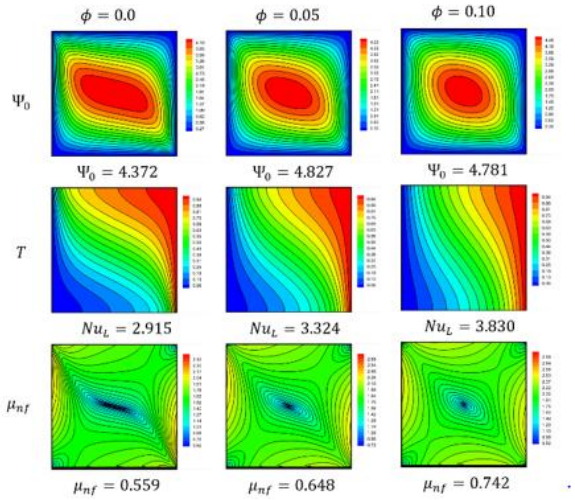

Fig 3. Contours of streamlines, Ψ_0, temperature, T, and nanofluid viscosity, μ_{nf} for R_T =200, n=1.2, Ha =1.0, Φ = 90°, ω = 0° and various values of ϕ.

Figure 3 displays the flow behaviorΨ_0 the isotherms T, and the apparent viscosity η_{nf} contours for the different values of carbon nanotubes loadings ϕ (0, 0.05 and 0.1). It is shown that a single cell is formed inside the entire cavity, but it is noticed that by adding 5% of carbon nanotube into the base fluid (water), the fluid flow intensity increases inside the cavity as mentioned by the $|\Psi|_{max}$ values. However, the addition of more SWCNT (0.05 and 0.10) reduces the fluid flow intensity to a value below of that recorded for the percentage of 5%, which is explained by the recorded increase in the apparent viscosity η_{nf} of the SWCNT-water nanofluid as seen in Fig. 3 (η_{nf}).Also, the increase of SWCNT percentage in the base fluid increases the convection rate and enhances the heat transfer inside the enclosure even with decrease of the fluid flow strength mentioned previously. This is due to the enhancement in the thermal conductivity by adding more carbon nanotubes (the effect of the enhancement of the thermal conductivity of the nanofluid due to the addition of more nanotubes overcomes the effect of the increasedapparent viscosity).

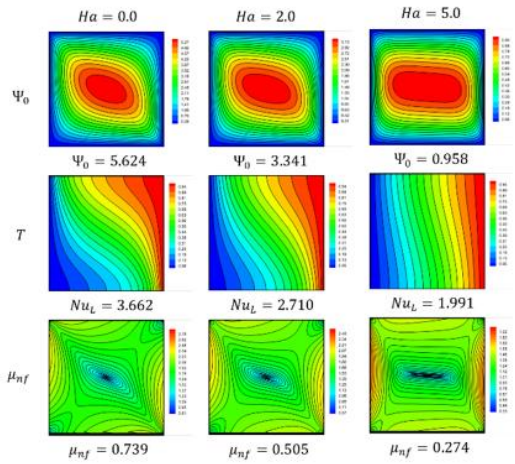

Fig 4. Contours of streamlines,Ψ_0, temperature, T, and apparent viscosity of nanofluid, μ_{nf}, for R_T =200, ϕ=0.05 n=1.2, Ha=1.0, Φ = 90°, ω = 0° and various values of Ha.

Figure 4 present the contours of streamlines,Ψ_0, temperature, T, and apparent viscosity of nanofluid, μ_{nf} obtained numerically for the different values of Hartman number Ha(0, 2 and 5) with power-law index of n = 1.2 and R_T = 200, ϕ =0.05, Φ = 90°, ω = 0°. The streamlines are uniformly distributed with designated increments, spanning from zero at the boundaries to the maximum value at the center. The isotherms are uniformly distributed between the successive positions of the peak temperature T_{max} situated lower edge of the right vertical wall. On the other hand, the minimum temperature T_{max} are situated along the upper edge of the left vertical wall. The apparent viscosity of nanofluid, represented by μ_{nf} lines, displays a uniform distribution from the center to the cavity edges. It can be observed in Figure 4 that asthe Hartmann number (Ha) increases, the values μ_{nf}decrease. For example, for Ha=0theμ_{nf}=0.739,Ha=2 theμ_{nf}=0.50 andHa=5theμ_{nf}=0.274.

Figure 5 present the contours of streamlines Ψ_0, the apparent viscosity, andμ_{nf}, temperature, T, and, for Rayleigh numberR_T =200, volume fraction of nanoparticlesϕ=0.05, and the inclination angle of the cavityΦ =90°,power-law index n=1.2, Hartmann numberHa=1.0 and ω=0°for different values of inclination angles, Φ, from 0° to 135°. We observed that in this figure the influence of Φ in the contours of stream function Ψ_0, temperature T, and apparent viscosityμ_{nf}. The streamlines exhibit a uniform distribution with specified increments, $\Delta\Psi$, peaking at

its maximum value, Ψ_{max}, near the center and diminishing to zero at the perimeters. The isotherms lines display a uniform distribution between the maximum temperature, T_{max}, and the minimum temperature, T_{min}, consequently, temperature gradients is notably attenuated with an increase inΦ. The apparent viscosity of nanofluid, represented by μ_{nf} lines, displays a uniform distribution from the center to the cavity edges. Specifically, μ_{nf} values are observed to be 0.696 for Φ = 45°, 0.520 for Φ= 135°.

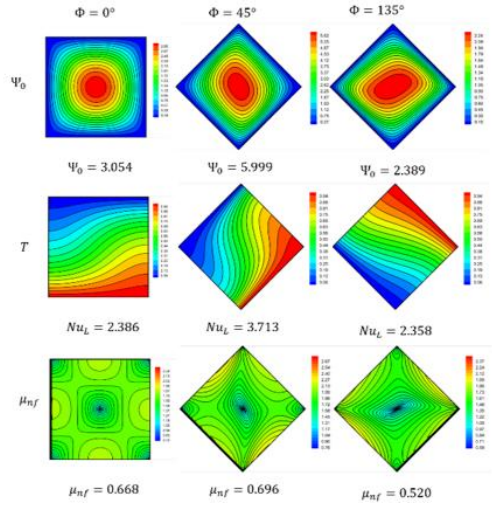

Fig 5. Contours of streamlines,Ψ_0, temperature, T, and apparent viscosity nanofluid, μ_{nf}, for R_T =200, ϕ=0.05 n=1.2, Ha =1.0, ω = 0° and various values of Φ.

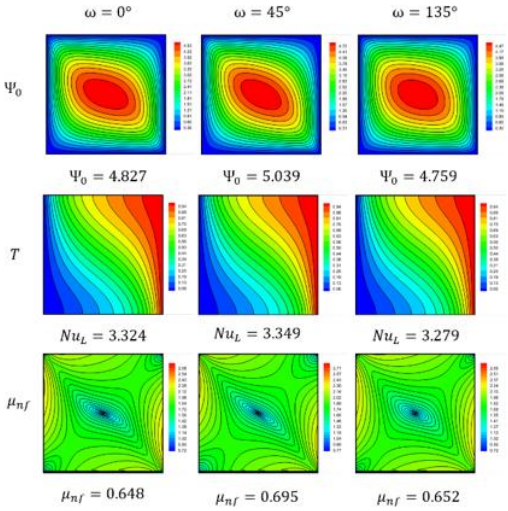

Fig 6. Contours of streamlines,Ψ_0, temperature, T, and apparent viscosity of nanofluid, μ_{nf}, for R_T =200, ϕ=0.05,Φ =90°, n = 1.2, Ha=1.0 and various values of ω.

Figure 6 present the contours of streamlines Ψ_0, temperature, T, and the apparent viscosity, μ_{nf}, for Rayleigh numberR_T =200, volume fraction of nanoparticlesϕ=0.05, and the inclination angle of the cavityΦ =90°, power-law index n=1.2, Hartmann numberHa=1.0 with Neumann-type boundary conditions. For different values of inclination angle of applied magnetic fieldω, (0°,45°,135°), respectively. Shows that the influence of the magnetic field inclination angle is negligible on the variation of the values of streamlines Ψ_0 , average Nusselt number Nu_L and apparent viscosityμ_{nf} .

4. Results and discussion

The objective of this study is to analyze the heat transfer performance of a non-Newtonian nanofluid (SWCNT-water) in an inclined saturated porous medium under the influence of a magnetic field. This is achieved by examining the relationships between the Rayleigh number R_T, nanoparticle volume fraction ϕ, inclination angle Φ, Hartmann number Ha, magnetic field inclination angle ω , and power-law index n. The numerical results reported in this study cover the ranges: $0 \leq R_T \leq 200$, $0 \leq \phi \leq 0.10$, $0° \leq \omega \leq 180°$, $0 \leq Ha \leq 10$, and $0° \leq \Phi \leq 180°$, $0.6 \leq n \leq 1.4$.

Figure 7 present apparent viscosity μ_{nf}profiles at the mid-width ($x = 0$), (a) influence of the power-law index n; (b) nanoparticle volumetric fractionϕ; (c) influence of Hartmann number Ha; and (d) influence of the inclination angle Φ , (e) influence of inclination angle of applied magnetic fieldon the profiles of $\mu_{nf}$for R_T = 200. The value μ_{nf} (a) increases until reaching the maximum value at the center of the cavity for non-Newtonian fluids (pseudo plastic n=0.6 and n=0.8) unlike for delaminating fluids (n=1.2 and n=1.4) decreases until reaching the minimum value at the center of the cavity, apparent viscosityμ_{nf} takes a constant value for Newtonian fluids, Fig 7((b)-(e)) the value of μ_{nf} is proportionalto the values ofnanoparticle volumetric fraction ϕ and Ha and Φ, ω. from the center until reaching the maximum value at the edges of the cavity.

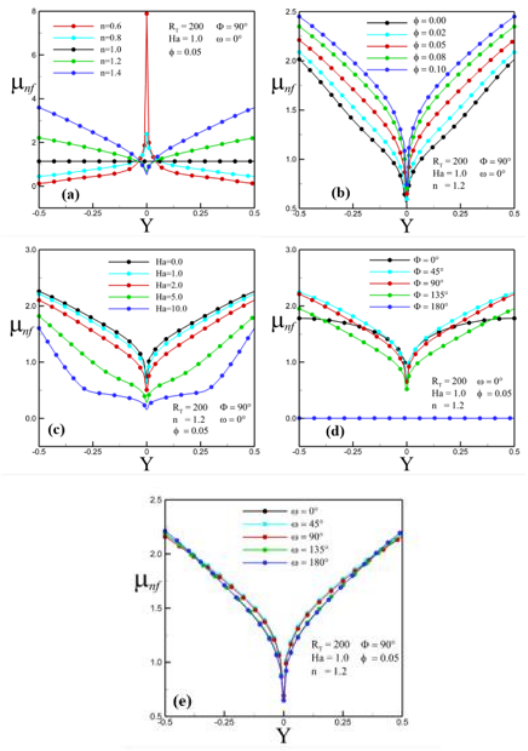

Fig 7. Apparent viscosity μ_{nf}profiles at the mid-width ($x = 0$): (a) influence of the power-law index n; (b) nanoparticle volumetric fraction ϕ; (c) influence of Hartmann number Ha; and (d) influence of the inclination angle Φ , (e) influence of inclination angle of applied magnetic field on the profiles of $\mu_{nf}$for R_T = 200.

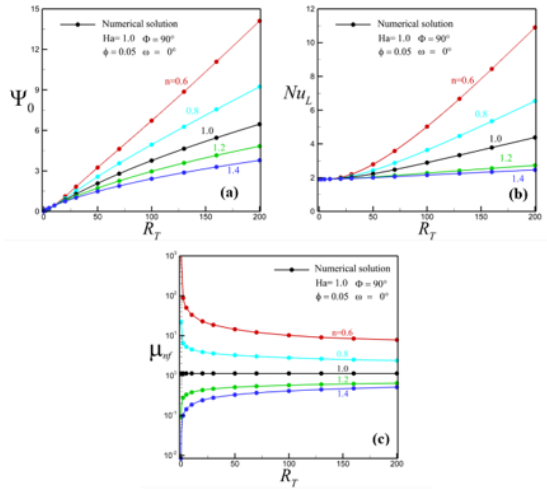

Fig 8. Variation of: (a) the stream functionΨ_0; (b) the average Nusselt number of the left wall; and (c) the apparent viscosity of the nanofluid with the Rayleigh number R_T and different values of the power-law index$n$ at Ha = 1, ϕ = 0.05, Φ = 90°and ω=0°.

Figure 8 present the variation of the stream functionΨ_0; the average Nusselt number of the left wall and the apparent viscosity of the nanofluid with the Rayleigh number R_T and different values of the power-law index n at Ha = 1, ϕ = 0.05, Φ = 90°and ω =0°. The value of streamlines Ψ_0 and the average Nusselt number Figs 8(a) and (b) increases proportionally with R_T for non-Newtonian fluids (pseudo plastic, delaminating) even for Newtonians. The increase appears significantly from the value R_T= 50, the value μ_{nf} increases proportionally with R_T for non-Newtonian delaminating fluids (n = 1.2, n = 1.4). Unlike for pseudo plastic (n = 0.6, n = 0.8). This change appears significantly over the interval of R_T (0-50), apparent viscosityμ_{nf} takes a constant value for Newtonian fluids.

Figure 9 present the variation of the stream functionΨ_0, the average Nusselt number of the left wall and the apparent viscosity of the nanofluid with the Rayleigh number R_T and different values of nanoparticle volumetric fraction ϕ for n =1.2, Ha = 1, Φ= 90°and ω=0°. The value of streamlinesΨ_0 Fig. 9(a) and the average Nusselt number,Nu and apparent viscosityμ_{nf}, Fig. 9((b) and (c)), increases proportionally with $R_T$and the volume fraction of nanoparticlesvalue. We found the sameΨ_0 profile with Alilat et al. [43].

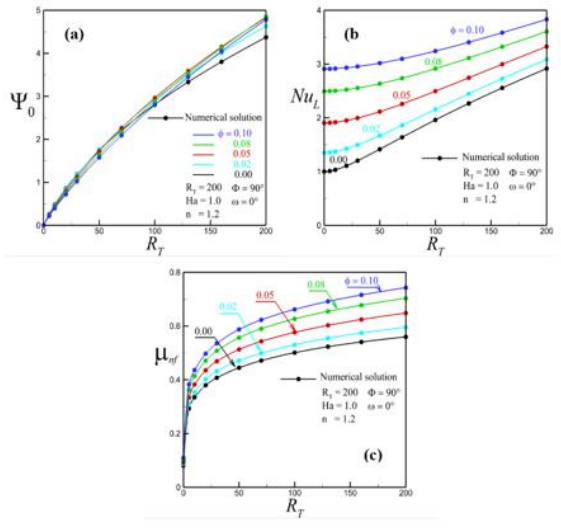

Fig 9. Variation of: (a) the stream functionΨ_0 , (b) the average Nusselt number of the left wall, and (c) the apparent viscosity of the nanofluid with the Rayleigh numberR_T and different values of nanoparticle volume fraction ϕ for n =1.2, Ha = 1, Φ = 90°and ω=0°.

Figure 10 present the variation of the stream functionΨ_0, the average Nusselt number of the left wall

Nu_L and the viscosity of the nanofluid $\mu_{nf}$with the Rayleigh number R_T and different values of Hartman number Ha for ϕ =0.05, n =1.2, Φ= 90°and ω=0°. The value of streamlinesΨ_0 and Nu_L Figs.10((a) and (b)), increase proportionally with Rayleigh number R_T. The more the value of Hartmann number Ha is decreased this increase appears if theHartmann number Ha take the values lower than 5. The same thing for nanofluid viscosityμ_{nf} Fig.10(c), but the increase is more sensitive on the interval ofRayleigh numberR_T lower than 75.

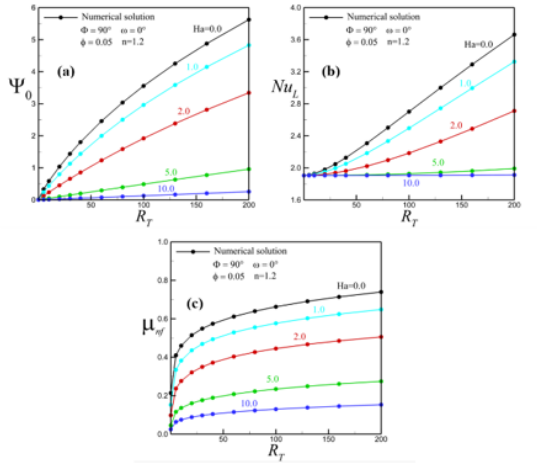

Fig 10. Variation of: (a) the stream functionΨ_0; (b) the average Nusselt number of the left wall Nu_L; and (c) the viscosity of the nanofluid $\mu_{nf}$with the Rayleigh number $R_T$and different values of Hartman number Ha forϕ =0.05, n = 1.2, Φ = 90°and ω=0°.

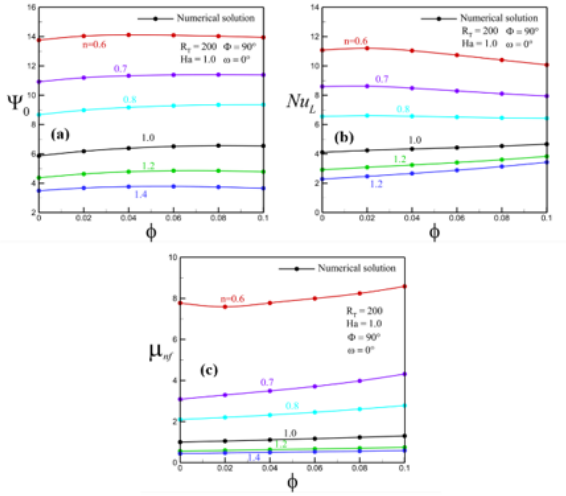

Fig 11. Variation of: (a) the stream functionΨ_0; (b) the average Nusselt number of the left wall Nu_L; and (c) the viscosity of the nanofluid $\mu_{nf}$with the nanoparticle volumetric fraction ϕ and different values of power-law index n for R_T=200, Ha = 1, Φ = 90°and ω=0°.

Figure 11 present the variation of the stream functionΨ_0, the average Nusselt number of the left wall Nu_L and the viscosity of the nanofluid $\mu_{nf}$with the nanoparticle volumetric fraction ϕ and different values of power-law index n for R_T =200, $Ha = 1$, Φ = 90°and ω=0°. The variation of the values of streamlinesΨ_0, the average Nusselt numberNu_Landapparent viscosityμ_{nf}, Figs. 11((a)-(c)), is negligible with the increase of the volume fraction of nanoparticles. But theΨ_0, Nu_L and μ_{nf} take the maximum values in non-Newtonian and pseudo-plastic fluids (n=0.6 and n=0.7) more than dilatant fluids (n=1.2 and n=1.4) and Newtonian fluids.

Figures 12 ((a) and (b)), the value of streamlines Ψ_0 and Nu_L is inversely proportional with Hartmann number Ha, the more the value of power-law index$n$ increases and this decrease appears clearly in the domain of Hartmann number Ha (0-4). As for the μ_{nf}. Fig.12(c) its value increases as Hartmann number Ha increases for pseudo-plastic non-Newtonian fluids (n=0.7 and n=0.8) and for dilatant and Newtonian fluids their changes are negligible.

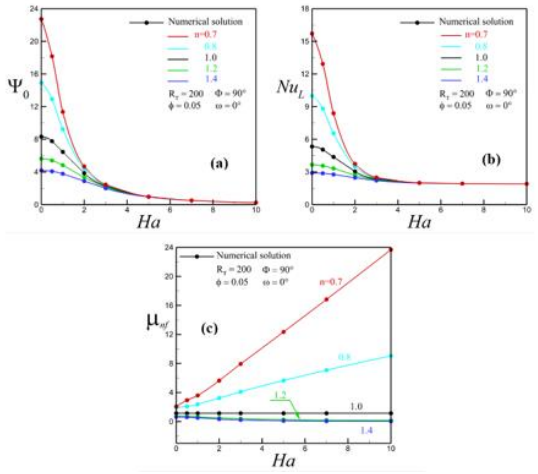

Fig 12. Variation of: (a) the stream functionΨ_0; (b) the average Nusselt number of the left wall Nu_L; and (c) the viscosity of the nanofluid μ_{nf} with the Hartman number$Ha$and different values of power-law index n for R_T =200,ϕ=0.05, Φ = 90° and ω=0°.

Figures 13(a)-(c), the value of streamlinesΨ_0 and apparent viscosityμ_{nf} is inversely proportional with Hartmann number Ha plus the value of nanoparticle volumetric fraction ϕ decreases, and for Nu_LFig.13(b) this decrease appears clearly in the domain of Hartmann number Ha (0-5). More than 5 the change of Ha is negligible.

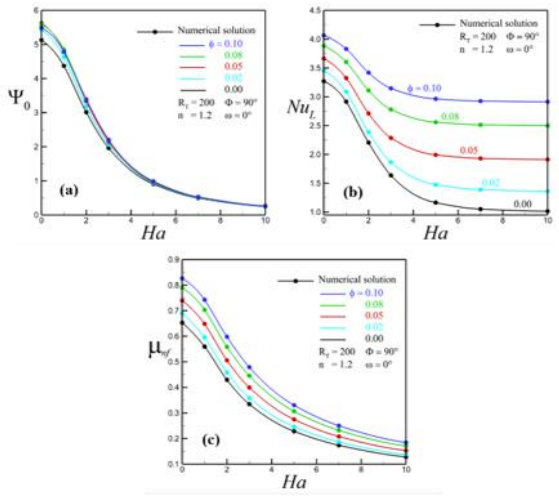

Fig 13. Variation of: (a) the stream functionΨ_0 ; (b) the average Nusselt number of the left wall Nu_L; and (c) the viscosity of the nanofluid μ_{nf} with the Hartman number$Ha$and different values of nanoparticle volumetric fraction ϕ for n =1.2, R_T =200, Φ= 90° and ω=0°.

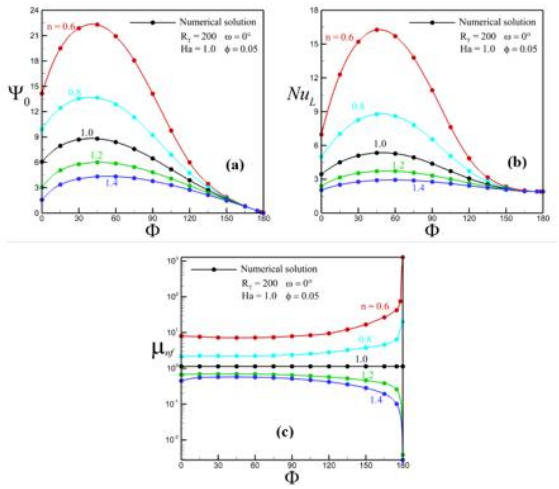

Fig 14. Variation of: (a) the stream functionΨ_0; (b) the average Nusselt number of the left wall Nu_L; and (c) the apparent viscosity of the nanofluid $\mu_{nf}$with the inclination angleΦ and different values of power-law index n forϕ =0.05, Ha=1, R_T =200 and ω=0°.

The influence of the inclination angle Φ on the values of streamlines$\Psi_0$andNu_L,Figs. 14((a) and (b)), is seen in the range of Φ = (0°-150°) whatever the type of fluid (Newtonian and non-Newtonian) they are increased up to the maximum value at Φ =45° after which they are decreased up to the minimum value at Φ =150°. As for the nanofluid viscosityμ_{nf} the variation of its value appears after an angle of 150° for non-Newtonian fluids (pseudo-plastic and dilatant), the inclination angle Φdoes not influence the value of μ_{nf} for Newtonian fluids.

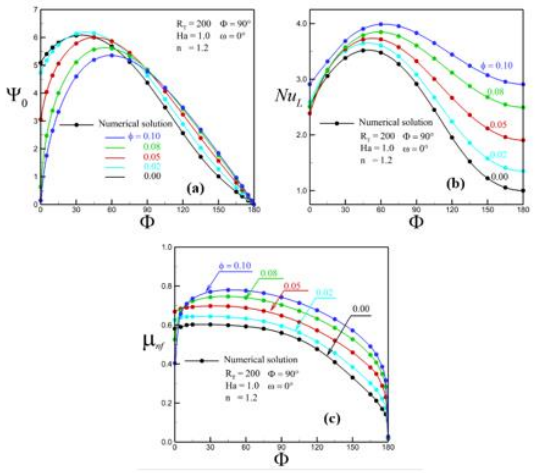

Fig 15. Variation of : (a) the stream functionΨ_0, (b) the average Nusselt number of the left wall Nu_L ; and (c) the apparent viscosity of the nanofluid μ_{nf} with the inclinaisant angleΦ and different values ofϕ for n=1.2,Ha=1, R_T=200 and ω=0°.

The influence of tilt angle Φ on the values of streamline$\Psi_0$and Nu_L, Figs.15((a) and (b)), is shown in the range of Φ = (0°-150°) for different volume fraction of nanoparticles in the fluid they are increased up to the maximum value at Φ ≈60°, after its the values of streamlines$\Psi_0$they are decreased up to 0 and for Nu_L up to the minimum value at Φ ≈165°. As for Fig.15(c)apparent viscosityμ_{nf}take the max value at Φ≈45° and this, the more the value of the volume fraction increases that's to say μ_{nf}in the angle 45° and fraction =0.10 sup to 0.08 and so on. After it's the values are decreased up to 0 at Φ≈180°.

The influence of the inclination angle Φ on the values of Ψ_0 and Nu_L, Fig.16((a) and (b)) is shown in the range of Φ = (0°-150°) for differentHartmann number Ha they are increased up to the maximum value at Φ ≈60° after its the values ofΨ_0 they are decreased up to 0 and for Nu_L up to the minimum value at Φ ≈165°. The maximum values of Ψ_0, Nu_L and nanofluid viscosityμ_{nf} at Ha=0 for fixed Φare increased to the maximum values for Ha=1 and the maximum values of streamlines Ψ_0, Nu and μ_{nf} at Ha=1 for fixed Φ are increased to the maximum values for Ha=2 and so on up to the minimum values at Ha=10. In other words, the more value of Ha increases at fixed Φ the values ofΨ_0, Nu and $\mu_{nf}$are decreased.

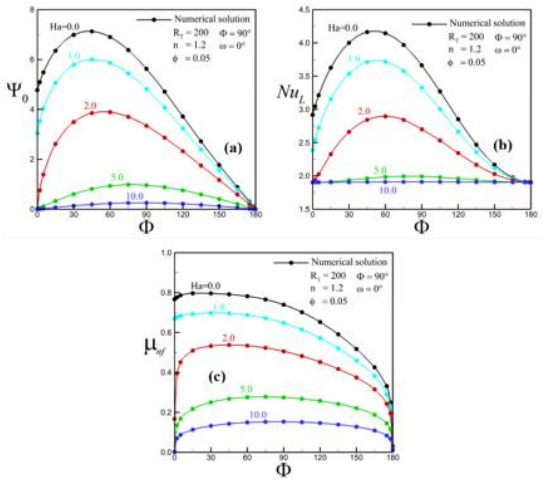

Fig 16. Variation of: (a) the stream functionΨ_0 (b) the Nusselt number of the left wall Nu_L; and (c) the viscosity of the nanofluid $\mu_{nf}$with the inclination angleΦ and different values of Ha forϕ =0.05, n=1.2, R_T=200 and ω=0°.

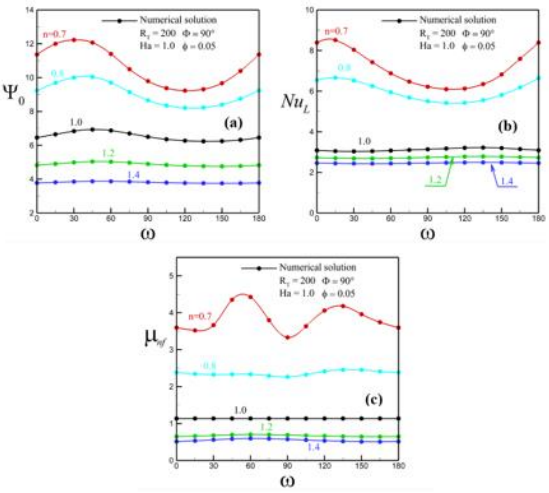

Fig 17. Variation of : (a) the stream function,Ψ_0 (b) the average Nusselt number of the left wall Nu_L; and (c) the apparent viscosity of the nanofluid $\mu_{nf}$with inclination angle of applied magnetic field$\omega$and different values of power-law index n for Ha =1, ϕ=0.05, R_T =200 andΦ =90°.

The influence of inclination angle of applied magnetic fieldω on the values ofΨ_0, Nu_L and μ_{nf}, Fig. 17((a)-(c)), appears in pseudo-plastic non-Newtonian fluids (n=0.7 and n=0.8) unlike other fluids (dilatant and Newtonian) the influence is negligible.

The variation of streamlines, Ψ_0, and apparent viscosityμ_{nf} as a function of inclination angle of applied magnetic field ω has different volume fractions in a sinusoidal way, Fig.18((a)-(c)), the influence of the inclination angle ω on the values of Nu_L has different volume fractions is negligible Fig. 18(b). The maximum values of streamlinesΨ_0,Nu_Landμ_{nf}at volume fraction ϕ =0.1 for fixed ω superior to maximum values for volume fraction ϕ=0.08 and the maximum values ofΨ_0, Nu_Landμ_{nf}at volume fraction ϕ=0.08 for fixed ω superior to maximum values for volume fraction ϕ =0.05 and so on up to the min values at volume fraction ϕ =0, 2. In other words, the more the value of volume fraction increases at fixed ω , the values of average Nusselt number Nu_L , and viscosity of the nanofluidμ_{nf}increase.

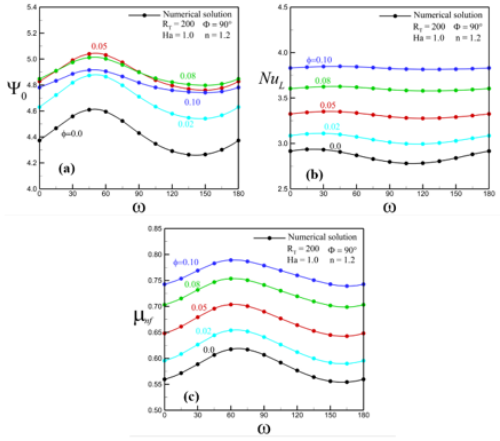

Fig 18. Variation of : (a) the stream function,Ψ_0; (b) the average Nusselt number of the left wall Nu_L and (c) the viscosity of the nanofluid μ_{nf} with inclination angle of applied magnetic field$\omega$and different values of nanoparticle volumetric fraction ϕ for n =1.2, Ha =1, R_T=200 andΦ =90°.

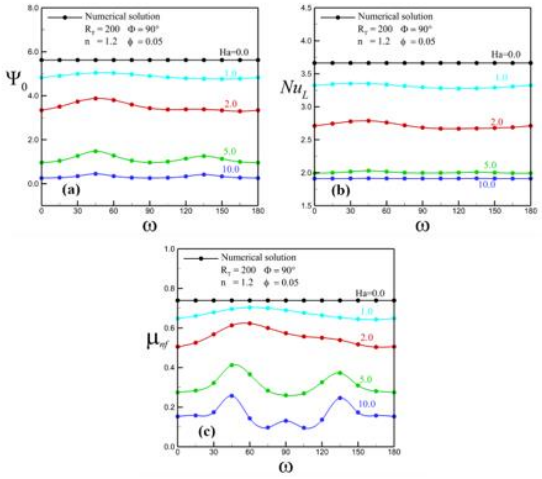

Fig 19. Variation of : (a) the stream function Ψ_0 (b) the average Nusselt number of the left wall Nu_L; and (c) the apparent viscosity of the nanofluid μ_{nf} with inclination angle of applied magnetic fieldω and

different values ofHartman number Ha forϕ =0.05, n =1.2, R_T =200 andΦ =90°.

Figure 19 present the contours of streamlines Ψ_0, the apparent viscosity, μ_{nf}, temperature, T, and, for Rayleigh number R_T =200, volume fraction of nanoparticles ϕ=0.05, and the inclination angle of the cavity Φ =90°, power-law index n=1.2, and ω=0°, for different values of Hartmann number Ha. We observed in this figure that the influence of inclination angle of applied magnetic field, ω, the values of $\Psi_0$and Nu_L, Fig.19((a) and (b)) at fixed the Hartmann number Ha, is negligible, but when the value of Ha increases, at fixed ω, the values of streamlines Ψ_0,average Nusselt number $Nu_L$and viscosity of the nanofluidμ_{nf}decrease.

5. Conclusion

This paper presents a numerical investigation of heat transfer involving non-Newtonian-based nanofluids within an inclined porous medium under the influence of MHD. The system was subjected to an inclined magnetic field affecting the dynamic viscosity. The enclosure featured differentially heated horizontal walls, while the vertical walls remained adiabatic. The power law model is used to analyze the behavior of non-Newtonian fluids and the Darcy model to describe the flow in the porous medium,the effect of the thermal Rayleigh number R_T, the power-law index n, Ha, the inclination angle of the cavity Φ, and the inclination angle of the magnetic field ω on the fluid flow and heat transfer rate.

The following briefly describes the primary finding of the current study:

- The study revealed a direct correlation between a decrease in the power-law index (n) and an increase in both convection strength Ψ_0, heat transfer rates (Nu_L), and Nano fluid viscosity μ_{nf}
- The variation of Ψ_0 and μ_{nf} and Nu_Las a function ofϕ. Note that as the value of ϕ increases from (0 to 0.1) theΨ_0, μ_{nf} and Nu_Lincrease.
- The influence of inclination angle of applied magnetic field ω on the values of $\Psi_0$and Nu_L, apparent viscosity μ_{nf} appears in pseudo-plastic non-Newtonian fluids (n=0.7 and n=0.8) unlike other fluids (dilatant and Newtonian) the influence is negligible.
- The value of Ψ_0 and apparent viscosity μ_{nf} is inversely proportional with Hartmann number, and for Nu_L this decrease appears clearly in the domain of Hartmann number Ha (0-5). More than 5 the change of Ha is negligible.
- The value of Ψ_0 and Nu_Lincrease proportionally with Rayleigh number R_T. The more the value of Hartmann number Ha is decreased this increase appears if the Hartmann number Ha take the values lower than 5. The same thing for nanofluid viscosity μ_{nf}, but the increase is more sensitive on the interval of Rayleigh number $R_T$lower than 75.
- Shows that an inclination angle of the cavity of 45° results in the maximum values of Ψ_0 and Nu_L and μ_{nf}.
- For a given value of Hartmann number Ha, the influence of inclination angle of applied magnetic fieldω on the values of streamlines$\Psi_0$and average Nusselt numberNu_L is negligible.

Refrences

[1] Vafai, K, and Tien, C. L. Boundary and inertia effects on flow and heat transfer in porous media. International Journal of Heat and Mass Transfer. (1981), 24(2), 195-203.
[2] Vafai K, and Hadim H. Overview of current computational studies of heat transfer in porous media and their applications- natural convection and mixed convection. Adv Numer Heat Transf. (2000), 2, 331–71.
[3] Chung S, Vafai K. Low-density lipoprotein transport within a multi-layered arterial wall-effect of the atherosclerotic plaque/ stenosis. J Biomech. (2013), 46, 574-85.
[4] Ai L, Vafai K. A. Coupling model for macromolecule transport in a stenosed arterial wall. Int J Heat Mass Transf. (2006), 49, 1568-91.
[5] Nield, D. A, and Bejan, A. (2006). Convection in porous media. Vol. 3, pp. 629-982. New York springer.
[6] Choi SUS. Enhancing thermal conductivity of fluids with nanoparticles. In: Proceedings of the ASME (1995), FED 231, MD 66. p. 99-105.
[7] Murshed SMS, Leong KC, and Yang C. Investigation of thermal conductivity and viscosity of nano fluids. Int J Therm Sci. (2008), 47, 560–8.

[8] Tiwari AK, Ghosh P, Sarkar J, Dahiya H, and Parekh J. Numerical investigation of heat transfer and fluid flow in plate heat exchanger using nanofluids. Int J Therm Sci. (2014), 85, 93-103
[9] Yu W, France DM, Routbort JL, and Choi SUS. Review and Comparison of Nano-fluid Thermal Conductivity and Heat Transfer Enhancements. Heat Transsf Eng. (2008), 29(5), 432–60
[10] Tiwari AK, Ghosh P, and Sarkar J. Particle concentration levels of various nano- fluids in plate heat exchanger for best performance. Int J Heat Mass Transf. (2015), 89, 1110–8.
[11] Saidur R, Leong KY, and Mohammad HA. A review on applications and challenges of nanofluids. Renew Sustain Energy Rev. (2011), 15, 1646–68
[12] Wang, X. Q, and Mujumdar, A. S. Heat transfer characteristics of nanofluids: a review. International journal of thermal sciences. (2007), 46(1), 1-19.
[13] Godson L, Raja B, Lal DM, and Wongwises S. Enhancement of heat transfer using nanofluids-an overview. Renew Sustain Energy Rev. (2010), 14, 629–41.
[14] Daungthongsuk W, and Wongwises S. A critical review of convective heat transfer of nanofluids. Renew Sustain Energy Rev. (2007), 11, 797–817
[15] Tiwari AK, Ghosh P, and Sarkar J. Heat transfer and pressure drop characteristics of CeO2/water nanofluid in plate heat exchanger. Appl Therm Eng. (2013), 57, 24-32.
[16] Tiwari AK, Ghosh P, and Sarkar J. Investigation of thermal conductivity and viscosity of nanofluids. J Environ Res Dev. (2012), 7(2), 768–77.
[17] Vajjha RS, and Das DK. A review and analysis on influence of temperature and concentration of nanofluids on thermophysical properties, heat transfer and pumping power. Int J Heat Mass Transf. (2012), 55, 4063–78.
[18] Chhabra, R.P, and Richardson, J.F. Non-Newtonian flow in the process industries: fundamentals and engineering applications. Butterworth-Heinemann, (1999).
[19] Yang, L, and Hu, Y. Toward TiO2 nanofluids-Part 2: applications and challenges. Nanoscale research letters. (2017), 12, 1-21.
[20] Pordanjani, A. H., Aghakhani, S., Afrand, M., Mahmoudi, B., Mahian, O, and Wongwises, S. An updated review on application of nanofluids in heat exchangers for saving energy. Energy Conversion and Management. (2019), 198, 111886.
[21] Minea, A.A. Advances in new heat transfer fluids: From numerical to experimental techniques. CRC Press, (2017).
[22] Mansour, M. A. A., Chamkha, A. J. J., Mohamed, R. A. A., Abd El-Aziz, M. M. M, and Ahmed, S. E. E. MHD natural convection in an inclined cavity filled with a fluid saturated porous medium with heat source in the solid phase. Nonlinear Analysis: Modelling and Control. (2010), 15(1), 55-70.
[23] Bühler, L., Mistrangelo, C, and Najuch, T. Magnetohydrodynamic flows in model porous structures. Fusion Engineering and Design, (2015), 98, 1239-1243.
[24] M'hamed, B., Sidik, N. A. C., Yazid, M. N. A. W. M., Mamat, R., Najafi, G, and Kefayati, G. H. R. A review on why researchers apply external magnetic field on nanofluids. International Communications in Heat and Mass Transfer. (2016), 78, 60-67.
[25] Nithyadevi, N, and Rajarathinam, M. Effect of Inclination Angle and Magnetic Field on Convection Heat Transfer for Nanofluid in a Porous Cavity. Journal of Applied Fluid Mechanics. (2016), 9(5), 2347-2358.
[26] Jahanbakhshi, A., Nadooshan, A. A, and Bayareh, M. Magnetic field effects on natural convection flow of a non-Newtonian fluid in an L-shaped enclosure. Journal of Thermal Analysis and Calorimetry. (2018), 133, 1407-1416.
[27] Pirmohammadi, M, and Ghassemi, M. Effect of magnetic field on convection heat transfer inside a tilted square enclosure. International Communications in Heat and Mass Transfer. (2009), 36(7), 776-780.
[28] Revnic, C., Grosan, T., Pop, I., et al. Magnetic field effect on the unsteady free convection flow in a square cavity filled with a porous medium with a constant heat generation. International Journal of Heat and Mass Transfer, (2011), vol. 54, no 9-10, p. 1734-1742.
[29] Wang, Z. H., Meng, X., & Ni, M. J. Liquid metal buoyancy driven convection heat transfer in a rectangular enclosure in the presence of a transverse magnetic field. International Journal of Heat and Mass Transfer. (2017), 113, 514-523.
[30] Shankar, B. M., Kumar, J, and Shivakumara, I. S. Magnetohydrodynamic stability of natural convection in a vertical porous slab. Journal of Magnetism and Magnetic Materials, (2017), 421, 152-164.
[31] Sheikholeslami, M. Numerical investigation for CuO-H2O nanofluid flow in a porous channel with magnetic field using mesoscopic method. Journal of molecular liquids. (2018), 249, 739-746.

[32] Kefayati, G. R. Simulation of heat transfer and entropy generation of MHD natural convection of non-Newtonian nanofluid in an enclosure. International Journal of Heat and Mass Transfer. (2016), 92, 1066-1089.
[33] Kefayati, G. R. Simulation of non-Newtonian molten polymer on natural convection in a sinusoidal heated cavity using FDLBM. Journal of Molecular Liquids, (2014), 195, 165-174.
[34] Kefayati, G. R. Lattice Boltzmann simulation of MHD natural convection in a nanofluid-filled cavity with sinusoidal temperature distribution. Powder Technology. (2013), 243, 171-183.
[35] Ali, F. H., Hamzah, H. K., Egab, K., Arıcı, M, and Shahsavar, A. Non-Newtonian nanofluid natural convection in a U-shaped cavity under magnetic field. International Journal of Mechanical Sciences, (2020), 186, 105887
[36] Aboud, E.D., Rashid, H.K., Jassim, H.M. Saba, Y. MHD effect on mixed convection of annulus circular enclosure filled with Non-Newtonian nanofluid. Heliyon, (2020), vol. 6, no 4, e03773.
[37] Motozawa M, Chang J, Sawada T, and Kawaguchi Y. Effect of magnetic field on heat transfer in rectangular duct flow of a magnetic fluid. Phys Proc. (2017), 9, 190–193.
[38] Javadpour, A., Najafi, M and Javaherdeh, K. Experimental investigation of forced convection heat transfer and friction factor of a non-Newtonian nanofluid flow through an annulus in the presence of magnetic field. Journal of the Brazilian Society of Mechanical Sciences and Engineering, (2018), 40, 1-12.
[39] Giwa, S. O., Sharifpur, M., Ahmadi, M. H, and Meyer, J.P. A review of magnetic field influence on natural convection heat transfer performance of nanofluids in square cavities. Journal of Thermal Analysis and Calorimetry. (2021), 145, 2581-2623.
[40] Kefayati, GHR. Simulation of mixed convection in a lid-driven cavity filled with non-Newtonian nanofluid in the presence of magnetic field. International Journal of Thermal Sciences, (2015), vol. 95, p. 29-46.
[41] Kumar, P. B, and Srinivas, S. Pulsating flow of a non-Newtonian nanofluid in a porous channel with magnetic field. Materials Today: Proceedings. (2019), 9, 320-332.
[42] Bennia, A, and Bouaziz, M. N. CFD modeling of turbulent forced convective heat transfer and friction factor in a tube for Fe3O4 magnetic nanofluid in the presence of a magnetic field. Journal of the Taiwan Institute of Chemical Engineers. (2017), 78, 127-136.
[43] Alilat, D., Alliche, M., Rebhi, Redha, et al. Inertial effects on the hydromagnetic natural convection of SWCNT-water nanofluid-saturated inclined rectangular porous medium. International Journal of Fluid Mechanics Research, 2020, vol. 47, no 5.
[44] Alilat, D, Rebhi, R, Alliche, M, and Chamkha, Ali J. Enhancement of dupuit-darcy thermal convection of swcnt-water non-newtonian nanofluid saturated porous medium. Heat Transfer Research. (2023), vol. 54, no 8, 29-59.
[45] Khir, S., Rebhi, R., Kezrane, M., and Borjini, M. N. Hysteresis and Bistability Bifurcation Induced by Combined Fluid Shear Thickening and Double-Diffusive Convection in Shallow Porous Enclosures Filled with Non-Newtonian Power-Law Fluids. East European Journal of Physics. (2024), 1, 203-220.
[46] [46] Khir, S., Henniche, R., Rebhi, R., Didi, F., and Kezrane, M. Bi-Stability Analysis of Double Diffusive Convection in A Tilted Square Porous Cavity Filled with A Non-Newtonian Power-Law Fluids. (2024), 20. 879-906. 10.62441/nano-ntp. v20i5.47.
[47] Garandet, J. P., Alboussiere, T, and Moreau, R. Buoyancy driven convection in a rectangular enclosure with a transverse magnetic field. International Journal of Heat and Mass Transfer, (1992), vol. 35, no 4, pp. 741-748.
[48] Tiwari, R.K and Kumar, D.M. Heat transfer augmentation in a two-sided lid-driven differentially heated square cavity utilizing nanofluids. International Journal of heat and Mass transfer, (2007), vol. 50, no 9-10, pp. 2002-2018.
[49] Xue, Q.Z. Model for thermal conductivity of carbon nanotube-based composites. Physica B: Condensed Matter, (2005), vol. 368, no 1-4, pp. 302-307.
[50] Maxwell, J.A. Treatise on Electricity and Magnetism, 2nd ed., Cambridge, UK: Oxford University Press, (1904).
[51] Jain, S, and Bhargava, R. Numerical simulation of free convection of MHD non-Newtonian nanofluid within a square wavy enclosure using Meshfree method. International Journal for Computational Methods in Engineering Science and Mechanics, (2020), vol. 22, no 1, pp. 32-44.
[52] Pascal, H. Rheological behaviour effect of non-Newtonian fluids on steady and unsteady flow through a porous medium. International Journal for Numerical and Analytical

Methods in Geomechanics, (1983), vol. 7, no 3, pp. 289-303.
[53] Pascal, H. Rheological effects of non-Newtonian behavior of displacing fluids on stability of a moving interface in radial oil displacement mechanism in porous media. International journal of engineering science, (1986), vol. 24, no 9, pp. 1465-1476.
[54] Peaceman, D.W, Rachford, J.R, and Henry H. The numerical solution of parabolic and elliptic differential equations. Journal of the Society for industrial and Applied Mathematics, (1955), vol. 3, no 1, pp. 28-41.
[55] Walker, K.L, and Homsy, G.M. Convection in a porous cavity. Journal of Fluid Mechanics, (1978), vol. 87, no 3, pp. 449-474.
[56] Bejan, A. On the boundary layer regime in a vertical enclosure filled with a porous medium. Letters in Heat and Mass Transfer, (1979), vol. 6, no 2, pp. 93-102.
[57] Beckermann, C., Viskanta, R., and Ramadhyani, S.A numerical study of non-Darcian natural convection in a vertical enclosure filled with a porous medium. Numerical heat transfer, (1986), vol. 10, no 6, pp. 557-570.
[58] Gross, R.J., Baer, M.R, and Hickox Jr, C.E. The application of flux-corrected transport (FCT) to high Rayleigh number natural convection in a porous medium. International Heat Transfer Conference Digital Library. Begel House Inc., (1986).
[59] Moya, S.L., Ramos, E, and Sen, Mihir. Numerical study of natural convection in a tilted rectangular porous material. International journal of heat and mass transfer, (1987), vol. 30, no 4, pp. 741-756.
[60] Manole, D.M. Numerical benchmark results for natural convection in a porous medium cavity. In: Heat and Mass Transfer in Porous Media, ASME Conference, (1992). pp. 55-60.
[61] Baytas, A.C, and Pop, I. Free convection in oblique enclosures filled with a porous medium. International Journal of Heat and Mass Transfer, (1999), vol. 42, no 6, pp. 1047-1057.
[62] Saied, N.H. and Pop, I. Non-Darcy natural convection in a square cavity filled with a porous media. Fluid Dyn. Res, (2005), vol. 36, no 1, pp. 35-43.